J Huazhong Univ Sci Technol［Med Sci］ 36(4):601-606,2016
DOI 10.1007/s11596-016-1632-5

Tuberous Sclerosis Complex: Imaging Characteristics in 11 Cases and Review of the Literature

Shan HU (胡 杉)[1], Dao-yu HU (胡道予)[2#], Wen-zhen ZHU (朱文珍)[2], Liang WANG (王 良)[2], Zi WANG (王 梓)[2]
1Department of Radiology, Guangdong General Hospital, Guangdong Academy of Medical Sciences, Guangzhou 510080, China
[2]Department of Radiology, Tongji Hospital, Tongji Medical College, Huazhong University of Science and Technology, Wuhan 430030, China

Summary: Tuberous sclerosis complex (TSC) is an uncommon multiorgan disorder that may present many and different manifestations on imaging. Radiology plays an important role in diagnosis and management, and can substantially improve the clinical outcome of TSC. Therefore, a comprehensive understanding of this disease is essential for the radiologist. The manifestations of TSC on computer tomography (CT) and magnetic resonance (MR) images were analyzed. Eleven patients with a clinical diagnosis of TSC were retrospectively reviewed. Central nervous system lesions included subependymal nodules (SENs) (11/11), subependymal giant cell astrocytomas (SEGAs) (2/11), cortical and subcortical tuber lesions (5/11), and white matter lesions (4/11). Of the 6 patients with abdominal scans, there were 6 cases of renal angiomyolipomas (AMLs), and one case of hepatic AMLs. Of the 4 patients undergoing chest CT, lung lymhangioleiomyomatosis (LAM) (2/4), and multiple small sclerotic bone lesions (2/4) were observed. Different modalities show different sensitivity to the lesion. Analysis of images should be integrated with patients' history in order to diagnose TSC.
Key words: tuberous sclerosis complex; computerized tomography; magnetic resonance imaging

Tuberous sclerosis complex (TSC), also known as Bourneville-Pringle syndrome, is an autosomal dominant neurocutaneous disorder, which is characterized by the formation of hamartomatous lesions in multiple organs. It has a prevalence of about 1:6000 newborns and affects approximately 1.5 million people worldwide, occurring in all races and both genders equally[1]. It is classically characterized by seizures, mental retardation and skin angiofibromas, although the full triad is seen only in 40% of the cases[2, 3]. The diagnostic criteria of the disease were defined by the 1998 consensus conference sponsored by the Tuberous Sclerosis Alliance and the National Institutes of Health (NIH). The criteria require TSC associated lesions of two or more organ systems or at least two dissimilar lesions of the same organ to confirm the diagnosis. The definite diagnosis is based on presentation of at least two major or one major plus two minor features. Probable diagnosis was due to presentation of one major and one minor feature. Possible diagnosis was according to presentation of one major or two or more minor features. The major changes involving skin include facial angiofibromas, hypomelanotic macules and shagreen patches; brain changes contain cortical tubers, subependymal nodules (SENs), subependymal giant cell astrocytomas (SEGAs) and retinal hamartomas; other organ manifestations include cardiac rhabdomyomas, renal angiomyolipoma (AML), pulmonary lymhangioleiomyomatosis (LAM). The minor features include multiple randomly distributed pits in dental enamel, rectal polyps, bone cysts, cerebral white-matter migration abnormalities on brain imaging, gingival fibromas, nonrenal hamartomas, retinal achromic patches, confetti skin lesions, and multiple renal cysts. DNA testing is available for diagnosis, but its accuracy is debated. Thus, examination of findings delivered by different imaging techniques has become an indispensable means for diagnosis and treatment of TSC. Therefore, it is important to familiarize ourselves with the imaging features of TSC.

In this retrospective study, we identify CT and MR imaging characteristics of 11 cases of TSC and put the findings in the context of existing literature.

1 MATERIALS AND METHODS

We searched picture achieving and communication system (PACS) of our department from January 1, 2010 to January 1, 2012. Keyword searches included the terms "TSC" and "renal angiomyolipoma (AML)", yielded a total of 36 cases. Two investigators (Shan HU and Zi WANG) independently reviewed the medical record including other organ clinical features, family history, operative records and pathological reports. In addition, radiological databases were also reviewed and analyzed. According to TSC diagnostic criteria (1992 revised edition), the case inclusion criteria were fulfilling the definite diagnosis of TSC, and the exclusion criteria were probable diagnosis, possible diagnosis of TSC and not TSC. Finally, 25 cases were excluded.

All the remaining 11 patients had undergone brain imaging, and 6 of them also had abdominal imaging and 4 chest imaging. Brain imaging included both CT and MRI scans in 2 cases (including diffusion-weighted cerebral MRI in 1 of them), CT only in 6 and MRI only in 3 cases (including contrast-enhanced scan for 1 of them).

Shan HU, E-mail: 27355432@qq.com
#Corresponding author, E-mail: cjr.hudaoyu@vip.163.com

Six of the 11 patients had also undergone abdominal imaging. Among them, 2 had both CT and MRI including MR liver acquisition with volume acceleration (LAVA) scan in 1 of them, CT only in 3 (including multi-phases enhancement) and only MR in 1 (including a diffusion-weighted and LAVA scans). All abdominal MRI scans used fat-saturation techniques.

CT and MR images were analyzed by two radiologists with 15 and 6 years of experience, respectively. They reached consensus on the analysis of the imaging manifestation of the lesion and reviewed the clinical data. The following imaging features were evaluated: type of lesions in multiple organs, number and size of lesions. Lesion appearance was compared between CT and MR images. Review of the patient charts was performed to assess demographic data (age, gender), clinical presentation, and final diagnosis.

2 RESULTS

2.1 Clinical Information

The demographic characteristics of the 11 patients (3 men, age range 3–54 years; mean age 18 years) are shown in table 1. Out of the 11, one case (1/11) presented with sudden unconsciousness and right limb weakness accompanied by vomiting. Nine patients (9/11) had history of epilepsy, two (2/11) reported headache and one (1/11) had mental retardation. Colic pain in the lumbar area was reported by three patients (3/11), of whom only one (1/3) had recurrent hematuria. Five patients (5/11) had multiple, discrete and reddish lesions over the cheeks and forehead (fig. 1).

Fig. 1 Multiple, discrete, reddish popular lesions over the cheeks in a 21-year-old female patient with colic pain in the lumbar area and recurrent hamaturia

Table 1 Demographics and presentation of 11 patients with TSC

Subjects	Age (years)	Gender	Clinical symptom
1	15	F	Headache and seizures
2	22	F	Colic pain in the lumbar area and seizure history
3	3	M	Seizure
4	5	M	Seizure
5	20	F	Headache and seizure history
6	22	F	Colic pain in the lumbar area and seizure history
7	54	F	Sudden unconsciousness and right limb weakness
8	4	F	Seizure
9	3	F	Seizure
10	33	M	Seizure and mental retardation
11	21	F	Colic pain in the lumbar area and recurrent hamaturia

F: female; M: male

2.2 Imaging Findings

The imaging characteristics are summarized in table 2. The brain lesions found in our patients included cortical tubers, SENs, SEGAs and white matter lesions. All cases had SENs on CT or MR images. Five patients showed cortical tubers and two patients presented with SEGAs, one of which was accompanied by hemorrhage. Four cases exhibited white matter lesions. Among abdominal lesions, renal AMLs were found in six cases while hepatic AMLs were only in one. Pulmonary LAMs and bone sclerotic lesions were shown on bone window in two patients.

Table 2 Radiologic characteristics of 11 cases of TSC

Multi-system	Characteristics	*n*
CNS	SENs	11/11
	SEGAs	2/11
	Cortical and subcortical tubers	5/11
	Whiter matter abnormalities	4/11
Abdomen	Liver AMLs	1/6
	Renal AMLs	6/6
Lung	LAMs	2/4
Bone lesions	Bone sclerosis	2/4

SEN: subependymal nodules; SEGA: subependymal giant cell astrocytomas; AML: angiomyoliopma

SENs, which appeared in all cases (11/11) in this study, are always found in the wall of the lateral ventricle. On MR images, SENs appear as irregular nodules, iso-intense on both T1- and T2-weighted images. However, SENs are usually hypo-intense to white matter on T2 images, due to the presence of calcifications. The calcified SENs showed high density on CT images (fig. 2D). By comparing SENs on CT and MR images, we found 8 lesions on MR images against 11 on CT images in case 5 of table 1, 4 lesions on MR images *vs*. 10 lesions on CT images in case 1 and 7 lesions on MR images *vs*. 11 lesions on CT images in case 6.

SEGAs, shown in two cases (2/11), are always found near the Monro foramina. T1- and T2-weighted imaging presented heterogeneous signal in SEGA of case 1 (table 1, fig. 3), indicating calcification and hemorrhage. It was iso-intense on T1-weighted images while hypo-intense on T2-weighted and fluid-attenuated inversion recovery (FLAIR) images, and demonstrated intense inhomogeneous enhancement. On CT image, the lesion was het-

erogeneous and of slightly high density calcification at its edge. The SEGA size was about 3 to 4 cm, and heavy hydrocephalus could be found (fig. 3). In case 5, the lesion showed inhomogeneously iso-intense signal on T1-weighted and FLAIR images and hypo-intense on T2-weighted images, with a size of about 1 to 1.5 cm with slight hydrocephalus.

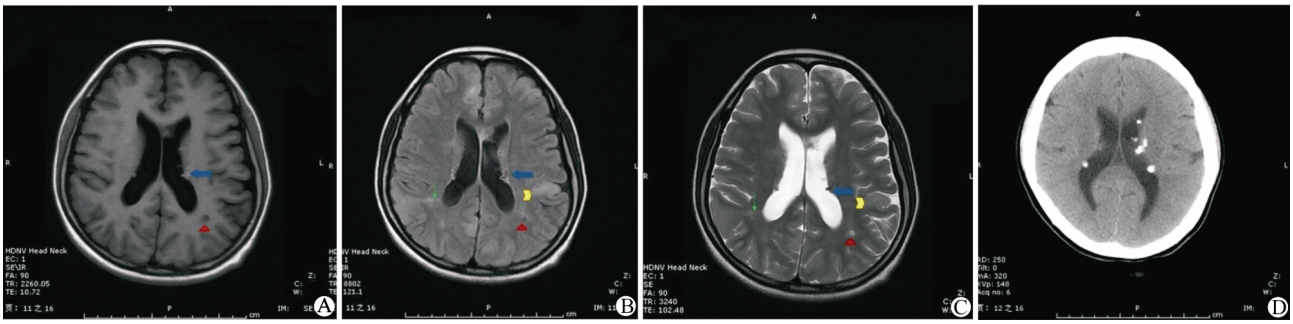

Fig. 2 The axial intracranial MR image

A: T1WI. The blue arrow shows the SENs are in the wall of lateral ventricle. Red triangle shows the cyst like white matter lesion. The white matter lesions and cortical and subcortical tubers are not displayed on T1WI. B: T2FLAIR. Green arrow exhibits radial white matter lesion. Yellow arrow head shows the cortical and subcortical tubers. C: T2WI. The SENs are hypointense on imaging. D: CT imaging. The calcified SENs show high density on CT imaging.

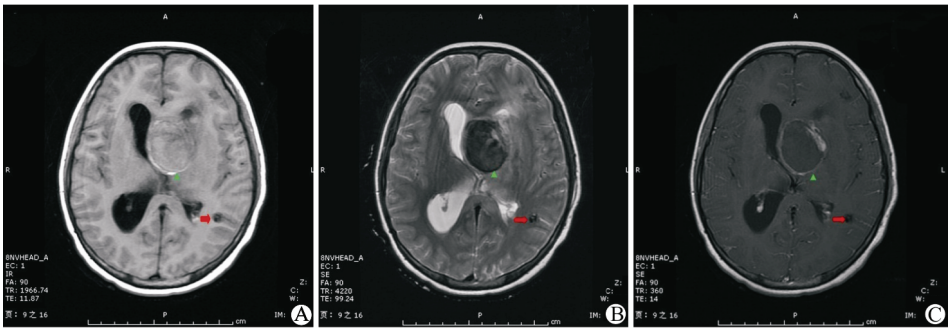

Fig. 3 SEGA on MRI

A: T2FLAIR, B: T2WI, C: T1WI with enhancement. SEGA (green arrow head) is found near the Monro foramina which manifests heterogeneous signal on T1- and T2- weighted imaging containing calcification and hemorrhage. The size of SEGA is 4 cm×3 cm with heavy hydrocephalus. Cortical and subcortical tuber with calcification is indicated by red arrows.

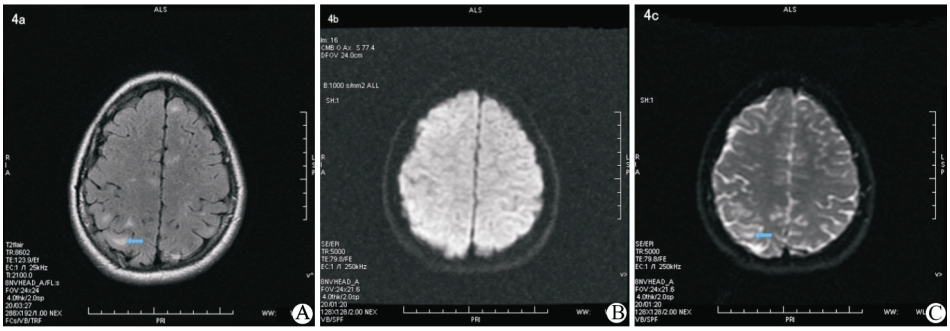

Fig. 4 Cortical and subcortical tubers on MRI

A: T2FLAIR. B: b=1000 mm^2/s diffusion weighted image (DWI). C: b=0 mm^2/s DWI. The cortical tubers (blue arrows) appear on the T2FLAIR and b=0 mm^2/s DWI

Cortical and subcortical tubers could not be found in any of the CT images (0/8), even in two cases tested with both CT and MRI scan. However, the lesions were all found in all five cases in MR images (5/5). The tubers showed iso-intense signal on T1- and hyper-intense on T2-weighted and FLAIR images in most cases, although in a few cases they were hypo-intense on T1- and T2-weighted and FLAIR images. In particular, lesions could be seen on DW images with b=0 mm^2/s, but they were invisible with b=1000 mm^2/s (fig. 2 and 4).

MRI is also better than CT in showing white matter abnormalities. White matter lesions were found in four cases (4/11) where they appeared as radiating lines of hyper-intensity extending from periventricular regions into the subcortical area on T2-weighted and FLAIR images (fig. 2B). Two of these cases also presented cyst-like lesions, which were hypo-intense on T1- and

hyper-intense on T2-weighted and FLAIR images (fig. 2C). The cyst-like lesions, both found adjacent to the lateral ventricle, had a diameter smaller than 1 cm.

Abdominal changes included renal and hepatic AMLs. Six patients (6/6) presented with renal AMLs, only one (1/6) showed liver AML. Two main radiographic features of renal AMLs were seen in our cases. Firstly, fat-contained AMLs were irregular shape of hyper-intensity with irregular shape on T1-weighted and were hypo-intense on fat-suppressed T2-weighted images; they could be seen in four cases (4/6). Secondly, lipid-poor lesions that showed a round shape of homogeneous iso-intensity on T1- and T2-weighted images, which were found in cases 6 and 11 (2/6) (fig. 5 and 6). Hepatic AMLs found in abdominal CT images were well circumscribed round areas with low attenuation consistent with presentation of fat.

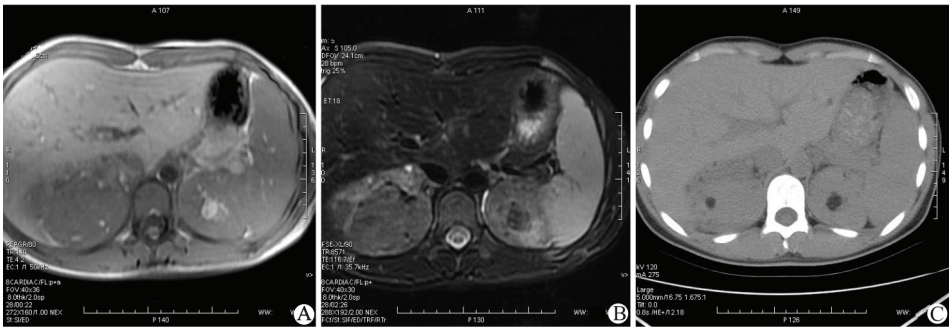

Fig. 5 The renal AMLs

A: T1WI; B: fat-suppressed T2WI. C: CT. The AMLs with lipid composition show hyperintense on T1WI on bilateral renals, but show hypointense on fat depressed sequence. On CT, the lesions show the round low attenuation signal.

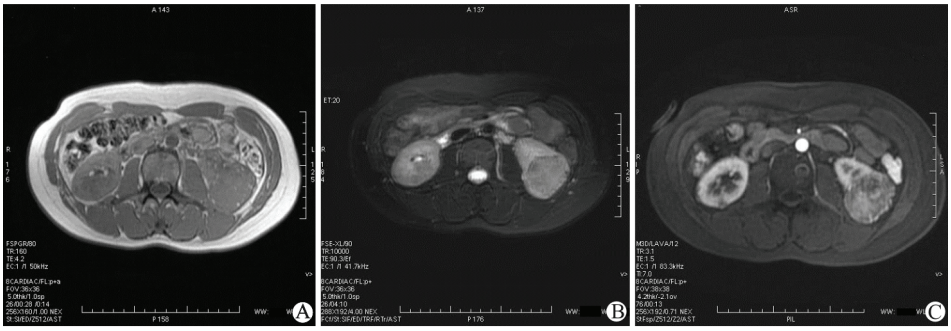

Fig. 6 The poor fat AMLs

A: T1WI. B: fat-suppressed T2WI. C: T1WI with enhancement. The homogeneous isointense tumors are found on bilateral kidneys without fat. On T1WI+contrast-enhanced imaging, the lesions show the inhomogeneous obvious enhancement.

The other manifestations included pulmonary LAMs and bone lesions. Lung LAMs appeared in two cases (2/4) in pulmonary CT scan, and they were multiple, bilateral and widespread thin wall cysts (fig. 7). Bone lesions (2/4) had two radiographic features: cyst-like lesions and sclerotic lesions which were round high attenuation in the bone window (fig. 8).

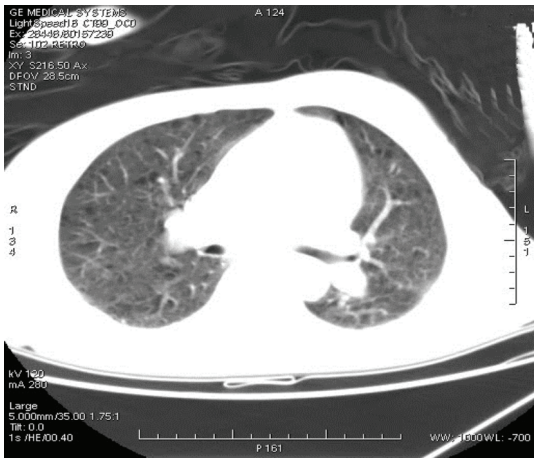

Fig. 7 The pulmonary LAMs

Multiple, bilateral and widespread thin wall cysts are found on chest CT.

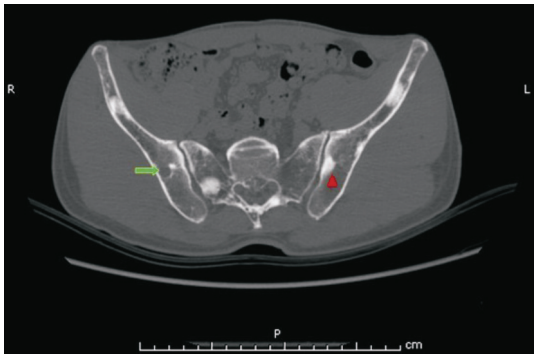

Fig. 8 The bone lesions

Red arrow shows the sclerotic lesion and green arrow shows the cyst lesion.

3 DISCUSSION

Our review showed that TSC is a disorder that may manifest itself in many and quite different ways on images with different modalities. Our cases have shown that

common brain lesions characterizing TSC include cortical tubers, SENs, SEGAs, and white matter lesions. Brain structural abnormalities can occur due to disturbed neural migration, which leads to changes in the number, size and thickness of the cortical gyri, heterotopia of neurons and structural disorder of cell layer of grey matter. Associated neurologic symptoms include seizures, autism, mental retardation and pervasive developmental disorder, learning and behavioral disorders[4].

The literature reports that SENs are present in about 80% of TSC patients. We found SENs in 100% of our cases. Histological studies have shown that SENs, which are covered by a thin layer of ependyma, contain both cells similar to the giant cells in tubers and elongated glial cells. SENs frequently show calcifications, particularly at an early stage[2]. SENs are typically less than 1 cm in size and better detected by CT than MRI.

SEGAs are generally found near the Monro foramina and accompanied with the development of non-communicating hydrocephalus. Although rare, they are WHO grade 1 tumors with slow growth, occurring in up to 26% of TSC patients[2]. SENs degenerate into SEGAs in 5%–10% of cases[5]. A useful set of criteria, adopted by Baron and Barkovich[6], define that a lesion with a diameter larger than 12 mm, inducing hydrocephalus, is suggestive of SEGA.

Cortical and subcortical tubers are cerebral cortical developmental malformations. We found that MRI is a more sensitive modality than CT for the identification of cortical tubers. Moreover, lesions were better displayed on the T2-weighted and FLAIR images, where they were hyper-intense. Tubers were presented more clearly on diffusion-weighted images with b=0 mm^2/s than in those with higher b values. Gallagher *et al*[7] showed that the tubers can be classified into three types according to the MRI signal intensity of their subcortical white matter component. Type A is isointense on T1-weighted images and hyper-intense in T2-weighted and FLAIR images; type B is hypointense in T1-weighted images and homogeneously hyperintense on T2-weighted and FLAIR images; type C is hypointense on T1-weighted images, hyperintense on T2-weighted, and heterogeneous in FLAIR images, characterized by a hypointense central region surrounded by a hyperintense rim. Due to the limited number of our cases, we only found two kinds of cortical and subcortical tubers: group A was iso-intense on T1- and hyper-intense on T2-weighted and FLAIR images; group B was hypo-intense on T1-weighted, T2-weighted and FLAIR images due to calcifications. Type B and C were not found in our cases. Ridler *et al*[8] reported that the number of lesions can be associated with epilepsy and autism and that tuber volume is on average larger in patients with a lifetime history of epilepsy. However, there was no correlation between intelligence quotient (IQ) and these measures of lesion load.

White matter lesions, known as unmyelinated white matter, consist of radial glial bands and periventricular cyst-like lesions. The radial glial bands were found more than the cyst-like lesions in our cases. According to Baskin[1], the bands are present in more than 80% of TSC patients and represent heterotophic neuronal and glial elements that arrested during cortical migration. For the cyst-like lesions, we found only two cases all located in the trigon of the lateral ventricle. Radhakrishnan and Verma[3] reported that cysts, frequently smaller than 1 cm, are present in approximately 44% of patients with TSC, and are located adjacent to the occipital horn or trigon of the lateral ventricle. The likely pathogenesis would be perivascular space enlargement, neuroepithelial cysts, or glial cysts. Enlarged perivascular space is seen on MR images as round, oval, or linear structures with signal intensity similar to the one of cerebrospinal fluid spaces along the course of penetrating arteries[9].

TSC abdominal changes including renal complications and hepatic manifestations appeared in our cases. Renal AML is an uncommon benign tumor, which consists of fat, abnormal blood vessels and smooth muscle elements in varying proportions. Many clinicians believe that all AMLs must have detectable adipose tissue. Nevertheless, some AMLs exhibit poor fat content. Among our cases, two lacked enough reliable information to demonstrate adipose tissue in some masses, and one of the two cases had heterogeneous enhancement induced misdiagnosis. Low fat AMLs consist predominantly of spindle cells, along with epithelioid cells or vascular elements. The contribution of each of the different cell components can vary from lesion to lesion, and some lesions can exhibit a dominant cell type[10]. Low fat AMLs can be seen also in oncocytomas and renal carcinomas. Therefore, imaging features of poor fat content AML are prone to inducing misdiagnosis. Fortunately, fat-suppression techniques are now easily available in MRI. A careful comparison of images obtained with and without fat-suppressed sequences is very important for an accurate diagnosis of low-fat AMLs. In addition, grow rate has been proposed as a possible method to distinguish renal cell carcinomas from fat poor AMLs[11]. As most renal cell carcinomas (RCCs) with fat densities show calcification, fat-containing lesions with calcification favor a diagnosis of RCC rather than AML and this should be recommended for the surgeon. Homogeneous tumor enhancement and prolonged enhancement patterns on biphasic helical CT may be useful for differentiating AML with minimal fat content from RCCs[11]. Patient history may help to identify AMLs, especially for those which are not sporadic. Hepatic AMLs are histologically similar to renal AMLs. Therefore, the imaging features are very similar. On CT these lesions are well circumscribed round areas with low attenuation, consistent with fat presence. Hepatic AMLs associated with TSC are rare, accounting for 6%–25% of cases, as our results showed[12].

As to the pulmonary lesions, LAM is a rare disease that affects young women of child-bearing age. Two of our patients were found to have LAMs. Multi-slice spiral CT is sensitive to the pulmonary lesions. On chest CT images, multiple, bilateral and widespread thin-wall cysts were found. Cysts are usually 2–5 mm but can be as large as 25–30 mm in size. Cysts are typically round or ovoidal. Small centrilobular nodules, corresponding to hyperplastic muscle or pneumocyte hyperplasia, have been reported[13]. Pulmonary LAMs are characterized by progressive widespread proliferation of smooth muscle throughout the perilymphatic, peribronchiolar, and perivascular regions of the lungs[14].

In addition, cardiac rhabdomyoma occurs in at least 60% of children with TSC, but it was not found in our cases. Patients with these tumors sometimes are asyptomatic, but some patients may present with

Wolff-Parkinson-White syndrome (WPW), which is reported to be associated with TSC. A recent review suggested that 9%–13% of patients with rhabdomyomata have the WPW syndrome[15].

To sum up, TSC is an uncommon multiorgan disorder that may present itself with many and different manifestations on imaging scan. Some image manifestations can easily be confused with other diseases. The findings in our review suggest that the patient clinical features, family history and all multiorgan images should be fully integrated. Radiology plays an important role in diagnosis and management, and can substantially improve the clinical outcome of TSC. Therefore, a comprehensive understanding of this disease is essential for the radiologist.

Conflict of Interest Statement

We declare that we have no financial and personal relationships with other people or organizations that can inappropriately influence our work; there is no professional or other personal interest of any nature or kind in any product, service and/or company that could be construed as influencing the position presented in, or the review of, the manuscript entitled.

REFERENCES

1 Baskin HJ Jr. The pathogenesis and imaging of the tuberous sclerosis complex. Pediatr Radiol, 2008, 38(9):936-952
2 Celenk P, Alkan A, Canger EM, *et al.* Fibrolipomatous hamartoma in a patient with tuberous sclerosis: report of a case. Oral Surg Oral Med Oral Pathol Oral Radiol Endod, 2005,99(2):202-206
3 Radhakrishnan R, Verma S. Clinically relevant imaging in tuberous sclerosis. J Clin Imaging Sci, 2011,1:39
4 Maria BL, Deidrick KM, Roach ES, *et al.* Tuberous sclerosis complex: pathogenesis, diagnosis, strategies, therapies, and future research directions. J Child Neurol, 2004,19(9):632-642
5 Kalantari BN, Salamon N. Neuroimaging of tuberous sclerosis: spectrum of pathologic findings and frontiers in imaging. AJR Am J Roentgenol, 2008,190(5):W304-309
6 Baron Y, Barkovich J. MR imaging of tuberous sclerosis in neonates and young infants. AJNR Am J Neuroradiol 1999,20(5):907-916
7 Gallagher A, Grant EP, Madan N, *et al.* MRI findings reveal three different types of tubers in patients with tuberous sclerosis complex. J Neurol, 2010, 257(8):1373-1381
8 Ridler K, Suckling J, Higgins N, *et al.* Standardized whole brain mapping of tubers and subependymal nodules in tuberous sclerosis complex. J Child Neurol, 2004,19(9):658-665
9 Van Tassel P, Cure JK, Holden KR. Cystlike white matter lesions in tuberous sclerosis. AJNR Am J Neuroradiol, 1997,18(7):1367-1373
10 Dixon BP, Hulbert JC, Bissler JJ. Tuberous sclerosis complex renal disease. Nephron Exp Nephrol, 2011,118(1):e15-20
11 Shin NY, Kim MJ, Chung JJ, *et al.* The differential imaging features of fat-containing tumors in the peritoneal cavity and retroperitoneum: the radiologic-pathologic correlation. Korean J Radiol, 2010, 11(3):333-345
12 Chao CH, Lin CY, Chan SC, *et al.* Concurrent hepatic and ruptured renal angiomyolipoma in tuberous sclerosis complex. Chang Gung Med J, 2004,27(9):696-700
13 Seaman DM, Meyer CA, Gilman MD, *et al.* Diffuse cystic lung disease at high-resolution CT. AJR Am J Roentgenol, 2011,196(6):1305-1311
14 Castro M, Shepherd CW, Gomez MR, *et al.* Pulmonary tuberous sclerosis. Chest, 1995,107(1):189-195
15 O'Callaghan FJ, Clarke AC, Joffe H, *et al*. Tuberous sclerosis complex and Wolff-Parkinson-White syndrome. Arch Dis Child, 1998,78(2):159-162

(Received Mar. 25, 2015; revised June 12, 2016)